FULL PAPER

Single Metal Atoms Anchored in Two-Dimensional Materials: Bifunctional Catalysts for Fuel Cell Application

Seoin Back[a], Ambarish R. Kulkarni[a], Samira Siahrostami*[a]

Abstract: Single metal atoms doped in two-dimensional materials have attracted particular attention for various catalytic reactions, due to their unique properties beyond metal catalysts. Herein we present density functional theory (DFT) calculations to study a wide range of such systems for oxygen reduction reaction (ORR) and hydrogen oxidation reaction (HOR) for application in cathode and anode of fuel cell, respectively. We find that the scaling relation of adsorption free energies of relevant ORR intermediates changes in the direction of improved activity. By considering more than 50 combinations, various ORR and HOR candidates are identified with improved catalytic activities compared to the state-of-the-art Pt (111). Particularly, Rh embedded in N-doped graphene is predicted to be markedly active for bifunctional fuel cell catalysis. This work highlights the potential of these systems for various catalytic reactions and the importance of identifying new classes of electrocatalysts to alleviate the use of precious metals and to maximize the catalytic activity.

Introduction

Proton-exchange membrane fuel cell (PEMFC), a promising technology for automobile and stationary applications, converts the chemical energy of H_2 into electricity.[1] At the anode side of PEMFC, gaseous hydrogen is oxidized to generate protons and electrons, which are supplied to the cathode via membrane and external circuit, respectively, where oxygen is reduced to water. The sluggish oxygen reduction reaction (ORR) at cathode side, is the main bottleneck of PEMFC. Today, despite limited supply and cost, platinum-based catalysts remain the widely viable material for ORR due to their superior activity. Various Pt-based alloys,[2-4] core-shell structures[5-6] and nanostructure catalysts[7-9] have been extensively investigated to enhance Pt utilization and improve the intrinsic catalytic activity. Although the kinetics of hydrogen oxidation reaction (HOR) at the anode side is at least six orders of magnitude faster than that of cathodic reaction,[1] the use of Pt based catalysts holds back the large-scale commercialization of PEMFC. Therefore, to alleviate the use of costly Pt metal, designing a bifunctional active and Pt-free catalyst for both ORR and HOR is highly desirable.

Recent theoretical and experimental reports indicate that dispersed single metal atoms anchored in different supports are highly promising not only in minimizing the metal usage but also in introducing unique catalytic properties compared to their bulk metal counterparts.[10-12] Several experimental preparation methods have been suggested to prepare single atom catalysts (SACs). Using atomic layer deposition (ALD) technique, single Pd[13] and Pt[14] atoms have been synthesized in graphene substrate. The isolated single atoms have been identified by high-angle annular dark-field scanning transmission electron microscopy (HAADF-STEM) and X-ray absorption fine structure spectroscopy (XAFS). In addition, incipient wetness impregnation (IWI) method has been utilized to deposit Pt single atom on TiN and TiC nanoparticle supports.[15] These synthesized SACs have been tested for various catalytic reactions including hydrogenation/oxidation reactions of hydrocarbons[16-17], electrochemical oxygen reduction reaction[13-15, 18], hydrogen evolution reaction[19-20] and carbon dioxide reduction reaction[12, 21-22], and shown extraordinary catalytic activities compared to their corresponding bulk metal catalysts. Moreover, Au-doped graphene and Pt-doped carbon nanotube have been reported as ORR catalysts using theoretical calculations and shown to outperform Au(111)[23] and Pt(111)[10], respectively. From the electronic structure point of view, there are several beneficial properties in SACs, which result in extraordinarily different catalytic activities from metal bulk properties. Firstly, most of the SACs show high stability which comes from strong chemical bonding between single metal atom and substrate. Secondly, due to confinement of electrons and quantum size effects, discrete energy levels are formed around the Fermi level. Lastly, the unsaturated coordination environment of the single metal atom provides a fascinating active center with intriguing properties for catalysis.[24-25] In fact, the appropriate combination of metal and support could provide SACs with desired catalytic properties.[11, 18, 26-27]

In this work, we study a wide range of metals anchored in a number of two-dimensional materials and investigate their stability and activity for ORR/HOR. The two-dimensional substrates have high surface area and ability to trap and stabilize metal atoms in their naturally formed vacancies.[18, 28-29] Doping single metal atoms in these vacancies is a prevailing method to modify the electronic structure of rather inert two dimensional-materials and activate them for variety of reactions. [10-11, 22, 30] Herein, we focus on substitutional doping of metals in the single and double vacancies of the two-dimensional substrate. Extensive DFT calculations on transition metals[31-32], a wide range of oxides[33] and two-dimensional materials[28] revealed that the adsorption energies of ORR intermediates are linearly correlated. As a result, it is impossible to tune the binding energy of one intermediate without affecting the binding energy of the other, on any of these reported classes of materials. Herein we show that many of our examined metal-doped two-dimensional materials affect the adsorption energies of relevant ORR intermediates differently and go beyond the limitations followed on the previous reported classes of materials.[31-33] This in turn, allows to design ORR catalysts with higher activity. We further investigate their HOR activity and propose the best ORR/HOR bifunctional catalyst for fuel cell applications.

[a] Dr. Back, Dr. Kulkarni, Dr. Siahrostami
SUNCAT Center for Interface and Catalysis,
Department of Chemical Engineering
Stanford University
Stanford, CA 94305, United States
E-mail: samiras@stanford.edu

Supporting information for this article is given via a link at the end of the document.

Results and Discussion

Transition Metals Embedded in Two Dimensional Materials

Among various two-dimensional materials, we chose to investigate graphene, N-doped graphene, *h*-boron nitride, silicon carbide, silicene, and borophene (β_{12} and χ), which have been explored as support materials for various catalytic reactions (Figure 1).[29-30, 34-35] We note that for N-doped graphene, we only focus on pyridinic-N, which is one of the known N-types frequently found in the experimental samples although other structural effects could play roles in determining the catalytic activity.[36-38] Both single and double vacancies were considered for all materials except for borophene, which intrinsically has vacancy sites. Figure S1 and Table S1 show the calculated formation energies of transition metals embedded in the two-dimensional materials, referenced to the (defected) supports and the bulk metals[30] and the calculated dissolution potentials of metal atoms.[39] Using the most stable configurations with the most negative ΔE_{form}, we further investigate the ORR activity of SACs. We note that β_{12} and χ borophene do not sufficiently stabilize the metal atoms in most cases, thus they are excluded from further consideration.

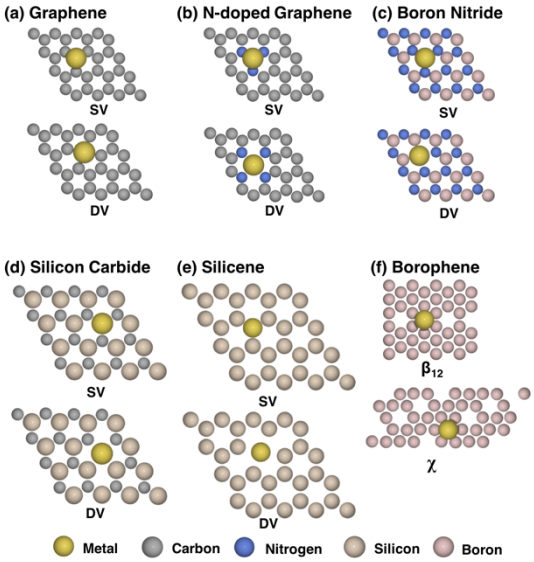

Figure 1. Optimized structures of single metal atom doped two-dimensional supports. Color code; C (*gray*), N (*blue*), B (pink), Silicon (*light brown*), metal (*yellow*).

ORR and HOR Activity of Single Atom Catalysts

To calculate the ORR activity we assume an associative reaction mechanism (eq. 1a to 1d) with *OOH, *O and *OH as intermediates.[40-41]

$$* + O_2(g) + (H^+ + e^-) \rightarrow *OOH \quad (1a)$$

$$*OOH + (H^+ + e^-) \rightarrow *O + H_2O(l) \quad (1b)$$

$$*O + (H^+ + e^-) \rightarrow *OH \quad (1c)$$

$$*OH + (H^+ + e^-) \rightarrow * + H_2O(l) \quad (1d)$$

The adsorption free energy of each intermediate is then calculated using CHE model (see computational details). The overall reaction free energy is set to thermodynamic value, 4.92 eV, to circumvent DFT error in describing the free energy of molecular O_2.[40, 42]

$$\Delta G_{O_2} = 4.92\ eV \quad (2a)$$

$$\Delta G_{*OOH} = G(*OOH) + \frac{3}{2}G(H_2) - G(*) - 2G(H_2O) \quad (2b)$$

$$\Delta G_{*O} = G(*O) + G(H_2) - G(*) - G(H_2O) \quad (2c)$$

$$\Delta G_{*OH} = G(*OH) + \frac{1}{2}G(H_2) - G(*) - G(H_2O) \quad (2d)$$

Using the calculated adsorption free energies of each ORR intermediate, we construct the free energy diagram for each individual studied catalyst. The effect of the electrode potential on the free energy of the intermediates is taken into account through shifting the electron energy by $-eU_{elec}$ where e and U_{elec} are the elementary charge and the electrode potential, respectively. The catalytic activity is evaluated on the basis of the calculated limiting potential (U_L), which is defined as the maximum potential at which all the steps become downhill in free energy. This theoretical basis has played a key role towards understanding the nature of active sites in a wide range of different structures[28], and has been used to guide catalyst design and optimization efforts[43-44] with a close correlation being made between the thermodynamics and kinetics for the ORR.[41, 45]

Figure 2(a) shows the calculated adsorption energies of *OOH (ΔG_{*OOH}) as a function of adsorption energies of *OH (ΔG_{*OH}) for the examined SACs. Also plotted are the known scaling relation reported for metals[31-32], oxide[32-33] and other classes of two-dimensional materials[28] (black dashed line) and ideal scaling relation (red dashed line). Interestingly, all SACs fall between the aforementioned two lines, and many of them are close to the ideal catalyst, which is marked with the red star. This implies that the overpotential of SACs could be further decreased compared to that of previously reported catalysts. The different scaling in the SACs is originated from their significantly different electronic structure. As shown in Figure S3 the projected density of states (PDOS) for the Pt atom in Pt (111), is very different from the one in Pt@SV, Pt@DV and Pt@N-DV-Gr. The *d*-states in Pt SACs are much more localized than Pt (111), and overlap with *s*- and *p*-states of neighboring C or N atoms indicate a strong interaction between support and single metal atom. This in turn, introduces a degree of covalent character in the binding of adsorbates, which could then alter the scaling behavior. We also note that in many cases, metal at single vacancies allow *OOH adsorbate to interact in a bidentate mode (Figure 3). This provides an extra degree of stabilization for *OOH adsorbate compare to *OH which results in different scaling from metals. On the other hand, metal atoms at double vacancies are found to adsorb *OOH in a monodentate mode, but they allow adsorbates to interact with support plane due to the less protrusion of metal atom (Table S2). Similar behavior has been observed on transition metal exchanged zeolites with cage-like rings.[46]

Figure 2(b), displays the ORR activity volcano plot for SACs compared to the known volcano for other classes of materials. [32] Interestingly, many SACs are positioned above the top of the conventional volcano, implying their high potential to be more active ORR catalysts. Particularly, $U_{L,ORR}$ of promising catalysts (*e.g.* Ni@DV-Gr, Pt@DV-Gr, Rh@N-DV-Gr) are 0.2 V higher than

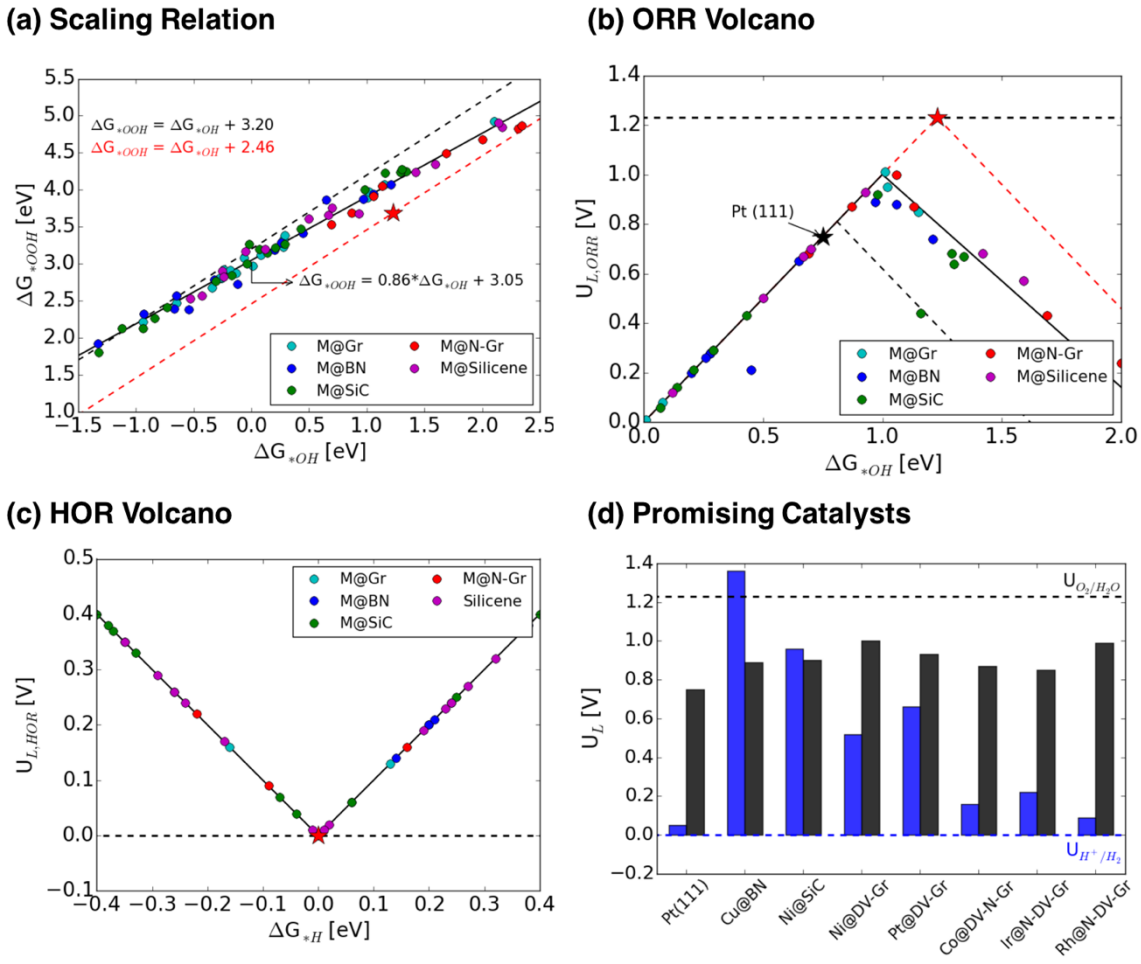

Figure 2. (a) The calculated ΔG_{*OOH} vs. ΔG_{*OH} over examined SAC systems. Black and red dashed lines are the universal scaling relation for metals and metal oxides[32-33] and the ideal scaling relation, respectively. (b) The ORR activity volcano plot as a function of ΔG_{*OH}. Black and red dashed volcano plots are based on the conventional and ideal scaling, respectively while a black solid volcano plot is based on the SAC scaling. Pt (111) is marked as a reference with a black star adapted from Ref. [4]. (c) The HOR activity volcano plot as a function of ΔG_{*H}. The ideal catalysts for ORR and HOR are marked with a red star. ORR and HOR volcanos containing all the data are shown in Figure S3. (d) A summary of limiting potentials of HOR (blue) and ORR (black). The dashed horizontal lines are equilibrium potential for ORR (U_{O_2/H_2O}= 1.23 V vs. RHE) and HOR (U_{H^+/H_2}= 0.00 V vs. RHE).

that of Pt (111), the best single element catalyst for ORR (Figure 2(d)). In addition to the ORR activity, we also calculated the formation free energy of *H (ΔG_{*H}) to investigate the HOR activity. We used ΔG_{*H} as a single descriptor to predict the theoretical limiting potential of HOR based on Heyrovsky-Volmer mechanism.[47-49] A large number of DFT calculations and experiments have found a strong correlation between ΔG_{*H} and HER activity, and suggested that catalysts with ΔG_{*H} close to 0 eV are promising candidates for HER reaction.[47-48, 50-51] Although HOR has received less attention compared to HER, it is generally accepted that good HER catalysts are also good HOR catalysts as a rule of thumb.[52] Furthermore, it was observed that a strength of *H binding is correlated with HOR overpotential on Pt surfaces.[49] Hence, we estimated HOR limiting potential using ΔG_{*H} as a single descriptor.

$$H_2(g) + * \rightarrow *H + H^+ + e^- \quad (3a)$$

$$*H \rightarrow * + H^+ + e^- \quad (3b)$$

We found that ΔG_{*H} spans from -1.0 eV to 2.0 eV on the different examined systems (Figure S2) and ΔG_{*H} is close to 0.0 eV in many cases, suggesting that SACs could outperform Pt catalysts in terms of HOR limiting potential. Using the limiting potential of ORR and HOR, we can then estimate the possibility of SACs for bifunctional fuel cell catalysts based on the fuel cell voltage as a descriptor ($U_{FuelCell}$=$U_{L,ORR}$− $U_{L,HOR}$). All the ORR and HOR limiting potentials and $U_{FuelCell}$ are summarized in Table S3. Among them, Co@N-DV-Gr, Ir@N-DV-Gr and Rh@N-DV-Gr showed 0.71, 0.63 and 0.90 V of $U_{FuelCell}$, respectively. Particularly, Rh@N-DV-Gr shows higher $U_{FuelCell}$ than Pt (111) ($U_{FuelCell} = 0.80\ V$), suggesting a

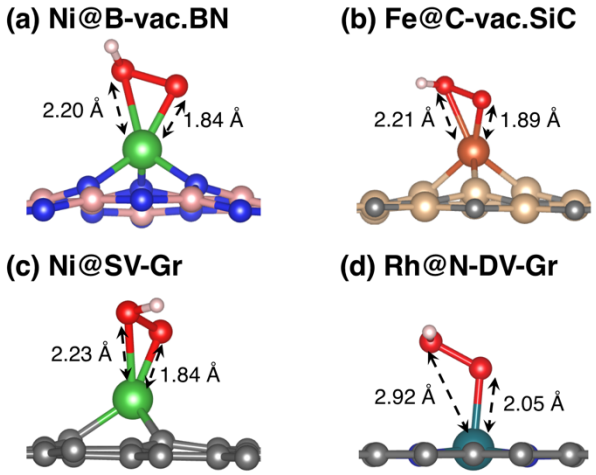

Figure 3. (a, b, c) The optimized geometries of bidentate *OOH adsorption on various supports with single vacancy. (d) As a comparison, monodentate *OOH adsorption on double vacancy support is also presented. Color code; C (*gray*), N (*blue*), Ni (*green*), Fe (*orange*), Rh (*turquoise*), H (*white*), Si (*light brown*).

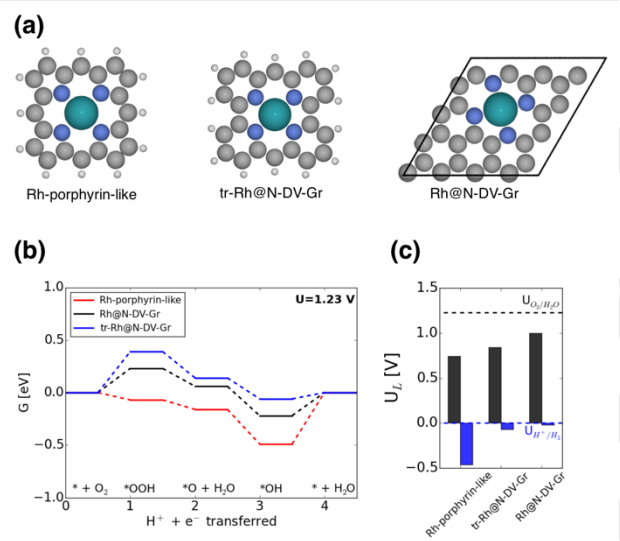

Figure 4. (a) The optimized geometries, (b) free energy diagrams for ORR at 1.23 V and (c) ORR (black) and HOR (blue) limiting potentials on Rh-N_4 catalysts with different local chemical environments. Color code; C (*gray*), N (*blue*), Rh (*turquoise*), H (*white*).

promising bifunctional fuel cell catalyst. Furthermore, the dissolution potential of Rh atom in Rh@N-DV-Gr is calculated to be 1.12 V, which is much larger than the calculated limiting potential (0.80 V). This suggests a high stability of Rh@N-DV-Gr under ORR condition (Table S1).

Local Coordination Dependence

Using the most promising Rh@N-DV-Gr, we investigated the effect of local chemical environment on the catalytic activity. Porphyrin like structure (Rh-porphyrin-like) and truncated Rh@N-DV-Gr (tr-Rh@N-DV-Gr) are characterized by the number of atoms outside the rings, and tr-Rh@N-DV-Gr and Rh@N-DV-Gr are characterized by the periodicity (Figure 4(a)). Figure 4(b) and (c) show that changing the number of atoms outside the rings significantly affects binding strengths of reaction intermediates, while the effect of the periodicity was relatively smaller. A distinct difference in energetics indicates that singly dispersed active sites are remarkably sensitive to the local chemical environment.

Benchmarking against HSE06

Keeping in mind that Rh@N-DV-Gr is a promising catalyst for ORR/HOR, we performed hybrid HSE06 calculations to validate the use of DFT-GGA. Figure 5(a) shows that all DFT-GGA functional energetics differ by less than 0.10 eV, and the limiting step is identical to (1d), while a bare HSE showed weaker binding of reaction intermediates (0.74 eV and 0.34 eV weaker than BEEF-vdW for *OOH and *OH, respectively) and, thus resulted in different limiting step (1a). However, the inclusion of implicit solvation correction (HSE_{solv}) led to a similar limiting potential and the same limiting step.

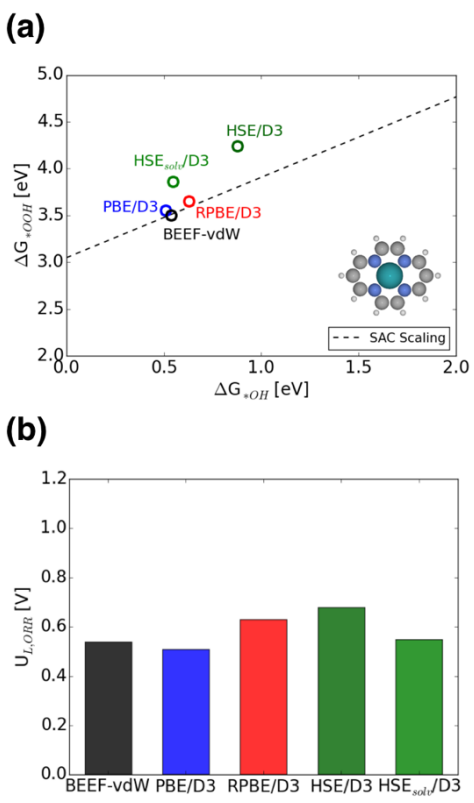

Figure 5. (a) Comparison of ΔG_{*OOH} vs. ΔG_{*OH} on Rh@N-DV-Gr cluster with different functionals. The dashed line is a scaling line of SACs in Figure 2(a). HSE_{solv} denotes an implicit solvation corrected HSE calculations. (b) Calculated U_{ORR} using different functionals.

Conclusions

In this work, using density functional theory calculations we studied the ORR activities for various metal atoms embedded in several two-dimensional materials to identify bifunctional fuel cell catalysts. We evaluated the stability of metal atoms in various support materials, and investigated ORR/HOR activity of stable combinations. Strong interactions between metal

atom and support affected the electronic structure of the single metal and altered the binding geometries of reaction intermediates, resulting in a higher catalytic activity. By considering both $U_{L,ORR}$ and $U_{L,HOR}$, we estimated the overall activity of new classes of catalysts for fuel cell applications. We identified Rh@N-DV-Gr as the best candidate with higher predicted $U_{FuelCell}$ than the best known single element catalyst, Pt. Although there are many different sites in experimentally synthesized SACs and different coordination environment of singly dispersed metal atoms may significantly affect the catalytic activity, this study highlights a high potential of SACs for heterogeneous catalysis. We also highlight that a search for new classes of catalysts should be continuously pursued to bypass the use of noble metal catalysts.

Theoretical Section

DFT calculations were performed using Quantum Espresso code[53] with ultrasoft pseudopotentials[54] through the Atomic Simulation Environment (ASE)[55]. We used the BEEF-vdW[56] exchange-correlation functional to accurately describe chemisorption as well as physisorption of metal-support complexes. The energy cutoff of the wavefunction and density were set to 500 and 5000 eV, respectively. All the supports are optimized using bulk unit cell with 12 × 12 × 1 Monkhorst-Pack *k*-points mesh, and then (4 × 4) supercells were utilized to calculate the binding energies of adsorbates with 4 × 4 × 1 *k*-points mesh. We added at least 15 Å vacuum in *z*-direction to decouple an artificial interaction between periodic images. All structures were fully relaxed until the total force becomes less than 0.05 eV/Å. The effect of solvation on polar adsorbates at water-solid interface was calculated using explicit water layer on Rh@N-DV-Gr structure. These calculations indicate that the solvation effect is very small (0.20 eV and 0.10 eV for *OH and *OOH, respectively) compared to the metal surfaces (0.50 eV and 0.25 eV).[40, 57] All calculations were performed spin polarized, although we found that the effect of spin polarization is marginal on the calculated adsorption energies (Figure S4). The optimized geometries of *O, *OH, *OOH adsorption are shown in Figure S5.

For the most promising candidate (Rh@N-DV-Gr), we benchmarked the GGA-level results (PBE/D3(BJ)[58-60], RPBE/D3(BJ)[59-61], BEEF-vdW[56]) against hybrid functional employing HSE06/D3(BJ)[59-60, 62] using Vienna Ab Initio Simulation Package (VASP)[63-64] with the projector-augmented wave (PAW) pseudopotential[65] and energy cutoff of 500 eV. We carried out single point calculations on the geometries optimized using BEEF-vdW. We further considered the effect of an implicit solvation using VASPsol[66] with a dielectric constant of solvent set to 78.4 for water. A small Rh@N-DV-Gr cluster was used to reduce a computational time (Figure 5a inset).

The calculated electronic energies were converted into free energies by adding zero-point energy, enthalpy and entropy corrections, which are calculated from a harmonic oscillator approximation at 300 K as implemented in ASE (Table S4). The computational hydrogen electrode (CHE) model was used to calculate the adsorption free energies of ORR intermediates.[40] In this model, the chemical potential of proton-electron pair is set to be equivalent to that of gas-phase H_2

$$H^+ + e^- \leftrightarrow \frac{1}{2}H_{2\,(g)}$$

and the effect of electrode potential is included by shifting the electron chemical potential by $-eU_{elec}$, where e and U_{elec} are the elementary charge and the electrode potential versus reversible hydrogen electrode (RHE), respectively. Therefore, the chemical potential of the proton and electron pair at potential U_{elec} can be estimated as follows;

$$G(H^+ + e^-) = \frac{1}{2}G(H_2) - eU_{elec}$$

Acknowledgements

S.B. acknowledges the support from Basic Science Research Program through the National Research Foundation of Korea (NRF) funded by the Ministry of Education (NRF-2017R1A6A3A03006971). S.B., A.K. and S.S. acknowledge the support from Toyota Research Institute.

Keywords: Single Atom Catalysts (SAC)• Oxygen Reduction Reaction (ORR)• Hydrogen Oxidation Reaction (HOR)• Two Dimensional Materials• Density Functional Theory (DFT) Calculations

References:

[1] M. K. Debe, *Nature* **2012**, *486*, 43-51.
[2] V. R. Stamenkovic, B. S. Mun, K. J. Mayrhofer, P. N. Ross, N. M. Markovic, *J. Am. Chem. Soc.* **2006**, *128*, 8813-8819.
[3] V. R. Stamenkovic, B. Fowler, B. S. Mun, G. Wang, P. N. Ross, C. A. Lucas, N. M. Marković, *Science* **2007**, *315*, 493-497.
[4] J. Greeley, I. Stephens, A. Bondarenko, T. P. Johansson, H. A. Hansen, T. Jaramillo, J. Rossmeisl, I. Chorkendorff, J. K. Nørskov, *Nat. Chem.* **2009**, *1*, 552-556.
[5] S. Back, Y. Jung, *ChemCatChem* **2017**, *9*, 3173-3179.
[6] A. L. Strickler, A. Jackson, T. F. Jaramillo, *ACS Energy Lett.* **2016**, *2*, 244-249.
[7] D. Wang, Y. Yu, H. L. Xin, R. Hovden, P. Ercius, J. A. Mundy, H. Chen, J. H. Richard, D. A. Muller, F. J. DiSalvo, *Nano Lett.* **2012**, *12*, 5230-5238.
[8] K. Jiang, Q. Shao, D. Zhao, L. Bu, J. Guo, X. Huang, *Adv. Func. Mater.* **2017**, *26*, 1700830.
[9] R. Chattot, T. Asset, P. Bordet, J. Drnec, L. Dubau, F. Maillard, *ACS Catal.* **2016**, *7*, 398-408.
[10] S. Siahrostami, G.-L. Li, J. K. Nørskov, F. Studt, *Catal. Lett.* **2017**, *147*, 2689-2696.
[11] J. Liu, M. Jiao, L. Lu, H. M. Barkholtz, Y. Li, Y. Wang, L. Jiang, Z. Wu, D.-j. Liu, L. Zhuang, *Nat. Commun.* **2017**, *8*, 15938.
[12] K. Jiang, S. Siahrostami, T. Zheng, Y. Hu, S. Hwang, E. Stavitski, Y. Peng, J. Dynes, M. Gangisetty, D. Su, *Energy Environ. Sci.* **2018**. DOI: 10.1039/C7EE03245E
[13] H. Yan, H. Cheng, H. Yi, Y. Lin, T. Yao, C. Wang, J. Li, S. Wei, J. Lu, *J. Am. Chem. Soc.* **2015**, *137*, 10484-10487.
[14] S. Sun, G. Zhang, N. Gauquelin, N. Chen, J. Zhou, S. Yang, W. Chen, X. Meng, D. Geng, M. N. Banis, *Sci. Rep.* **2013**, *3*, 1775.
[15] S. Yang, Y. J. Tak, J. Kim, A. Soon, H. Lee, *ACS Catal.* **2017**, *7*, 1301-1307.
[16] B. Qiao, A. Wang, X. Yang, L. F. Allard, Z. Jiang, Y. Cui, J. Liu, J. Li, T. Zhang, *Nat. Chem.* **2011**, *3*, 634-641.
[17] J. Lin, A. Wang, B. Qiao, X. Liu, X. Yang, X. Wang, J. Liang, J. Li, J. Liu, T. Zhang, *J. Am. Chem. Soc.* **2013**, *135*, 15314-15317.
[18] X. Zhang, J. Guo, P. Guan, C. Liu, H. Huang, F. Xue, X. Dong, S. J. Pennycook, M. F. Chisholm, *Nat. Commun.* **2013**, *4*, 2929.
[19] H. J. Qiu, Y. Ito, W. Cong, Y. Tan, P. Liu, A. Hirata, T. Fujita, Z. Tang, M. Chen, *Angew. Chem. Int. Ed.* **2015**, *54*, 14031-14035.

[20] N. Cheng, S. Stambula, D. Wang, M. N. Banis, J. Liu, A. Riese, B. Xiao, R. Li, T.-K. Sham, L.-M. Liu, *Nat. Commun.* **2016**, *7*, 13638.
[21] P. Su, K. Iwase, S. Nakanishi, K. Hashimoto, K. Kamiya, *Small* **2016**, *12*, 6083-6089.
[22] K. Jiang, S. Siahrostami, A. J. Akey, Y. Li, Z. Lu, J. Lattimer, Y. Hu, C. Stokes, M. Gangishetty, G. Chen, *Chem* **2017**, *3,* 950-960.
[23] S. Stolbov, M. Alcántara Ortigoza, *J. Chem. Phys.* **2015**, *142*, 154703.
[24] S. Back, J. Lim, N.-Y. Kim, Y.-H. Kim, Y. Jung, *Chem. Sci.* **2017**, *8*, 1090-1096.
[25] S. Back, Y. Jung, *ACS Energy Lett.* **2017**, *2*, 969-975.
[26] H. Zhang, S. Hwang, M. Wang, Z. Feng, S. Karakalos, L. Luo, Z. Qiao, X. Xie, C. Wang, D. Su, *J. Am. Chem. Soc.* **2017**, *139*, 14143-14149.
[27] C. Zhang, J. Sha, H. Fei, M. Liu, S. Yazdi, J. Zhang, Q. Zhong, X. Zou, N. Zhao, H. Yu, *ACS Nano* **2017**, *11*, 6930-6941.
[28] S. Siahrostami, C. Tsai, M. Karamad, R. Koitz, M. García-Melchor, M. Bajdich, A. Vojvodic, F. Abild-Pedersen, J. K. Nørskov, F. Studt, *Catal. Lett.* **2016**, *146*, 1917-1921.
[29] G. Elumalai, H. Noguchi, H. C. Dinh, K. Uosaki, *J. Electroanal. Chem.* **2017**. https://doi.org/10.1016/j.jelechem.2017.09.033
[30] C. Ling, L. Shi, Y. Ouyang, X. C. Zeng, J. Wang, *Nano Lett.* **2017**, *17*, 5133-5139.
[31] V. Viswanathan, H. A. Hansen, J. Rossmeisl, J. K. Nørskov, *ACS Catal.* **2012**, *2*, 1654-1660.
[32] I. E. Stephens, A. S. Bondarenko, U. Grønbjerg, J. Rossmeisl, I. Chorkendorff, *Energy Environ. Sci.* **2012**, *5*, 6744-6762.
[33] I. C. Man, H. Y. Su, F. Calle-Vallejo, H. A. Hansen, J. I. Martínez, N. G. Inoglu, J. Kitchin, T. F. Jaramillo, J. K. Nørskov, J. Rossmeisl, *ChemCatChem* **2011**, *3*, 1159-1165.
[34] K. J. Koski, Y. Cui, *ACS Nano* **2013**, *7*, 3739-3743.
[35] B. Feng, J. Zhang, Q. Zhong, W. Li, S. Li, H. Li, P. Cheng, S. Meng, L. Chen, K. Wu, *Nat. Chem.* **2016**, *8*, 563-568.
[36] H. Niwa, K. Horiba, Y. Harada, M. Oshima, T. Ikeda, K. Terakura, J.-i. Ozaki, S. Miyata, *J. Power Sources* **2009**, *187*, 93-97.
[37] C. V. Rao, C. R. Cabrera, Y. Ishikawa, *J. Phys. Chem. Lett.* **2010**, *1*, 2622-2627.
[38] J. W. To, J. W. D. Ng, S. Siahrostami, A. L. Koh, Y. Lee, Z. Chen, K. D. Fong, S. Chen, J. He, W.-G. Bae, *Nano Research* **2017**, *10*, 1163-1177.
[39] J. Greeley, J. K. Nørskov, *Electrochim. Acta* **2007**, *52*, 5829-5836.
[40] J. K. Nørskov, J. Rossmeisl, A. Logadottir, L. Lindqvist, J. R. Kitchin, T. Bligaard, H. Jonsson, *J. Phys. Chem. B* **2004**, *108*, 17886-17892.
[41] A. Kulkarni, S. Siahrostami, A. Patel, J. K. Nørskov, *Chem. Rev.* **2017** *118*, 2302-2312.
[42] J. Rossmeisl, A. Logadottir, J. K. Nørskov, *Chem. Phys.* **2005**, *319*, 178-184.
[43] J. K. Nørskov, T. Bligaard, J. Rossmeisl, C. H. Christensen, *Nat. Chem.* **2009**, *1*, 37-46.
[44] M. Mavrikakis, B. Hammer, J. K. Nørskov, *Phys. Rev. Lett.* **1998**, *81*, 2819.
[45] H. A. Hansen, V. Viswanathan, J. K. Nørskov, *J. Phys. Chem. C* **2014**, *118*, 6706-6718.
[46] S. Siahrostami, H. Falsig, P. Beato, P. G. Moses, J. K. Nørskov, F. Studt, *ChemCatChem* **2016**, *8*, 767-772.
[47] J. Greeley, T. F. Jaramillo, J. Bonde, I. Chorkendorff, J. K. Nørskov, *Nat. Mater.* **2006**, *5*, 909-913.
[48] J. K. Nørskov, T. Bligaard, A. Logadottir, J. Kitchin, J. G. Chen, S. Pandelov, U. Stimming, *J. Electrochim. Acta* **2005**, *152*, J23-J26.
[49] W. Sheng, Z. Zhuang, M. Gao, J. Zheng, J. G. Chen, Y. Yan, *Nat. Commun.* **2015**, *6*, 5848.
[50] J. Kibsgaard, C. Tsai, K. Chan, J. D. Benck, J. K. Nørskov, F. Abild-Pedersen, T. F. Jaramillo, *Energy Environ. Sci.* **2015**, *8*, 3022-3029.
[51] Z. W. Seh, K. D. Fredrickson, B. Anasori, J. Kibsgaard, A. L. Strickler, M. R. Lukatskaya, Y. Gogotsi, T. F. Jaramillo, A. Vojvodic, *ACS Energy Lett.* **2016**, *1*, 589-594.
[52] J. Greeley, N. M. Markovic, *Energy Environ. Sci.* **2012**, *5*, 9246-9256.
[53] P. Giannozzi, S. Baroni, N. Bonini, M. Calandra, R. Car, C. Cavazzoni, D. Ceresoli, G. L. Chiarotti, M. Cococcioni, I. Dabo, *J. Phys. Condens. Matter* **2009**, *21*, 395502.
[54] D. Vanderbilt, *Phys. Rev. B* **1990**, *41*, 7892.
[55] S. R. Bahn, K. W. Jacobsen, *Comput. Sci. Eng.* **2002**, *4*, 56-66.
[56] J. Wellendorff, K. T. Lundgaard, A. Møgelhøj, V. Petzold, D. D. Landis, J. K. Nørskov, T. Bligaard, K. W. Jacobsen, *Phys. Rev. B* **2012**, *85*, 235149.
[57] Z.-D. He, S. Hanselman, Y.-X. Chen, M. T. Koper, F. Calle-Vallejo, **2017**, *8*, 2243-2246.
[58] J. P. Perdew, K. Burke, M. Ernzerhof, *Phys. Rev. Lett.* **1996**, *77*, 3865.
[59] S. Grimme, J. Antony, S. Ehrlich, H. Krieg, *J. Chem. Phys.* **2010**, *132*, 154104.
[60] S. Grimme, S. Ehrlich, L. Goerigk, *J. Comput. Chem.* **2011**, *32*, 1456-1465.
[61] B. Hammer, L. B. Hansen, J. K. Nørskov, *Phys. Rev. B* **1999**, *59*, 7413.
[62] A. V. Krukau, O. A. Vydrov, A. F. Izmaylov, G. E. Scuseria, *J. Chem. Phys.* **2006**, *125*, 224106.
[63] G. Kresse, J. Furthmüller, *Comput. Mater. Sci.* **1996**, *6*, 15-50.
[64] G. Kresse, J. Hafner, *Phys. Rev. B* **1993**, *48*, 13115.
[65] P. E. Blöchl, *Phys. Rev. B* **1994**, *50*, 17953.
[66] K. Mathew, R. Sundararaman, K. Letchworth-Weaver, T. Arias, R. G. Hennig, *J. Chem. Phys.* **2014**, *140*, 084106.

Entry for the Table of Contents (Please choose one layout)

Layout 1:

FULL PAPER

Single metal atoms anchored in two-dimensional materials are interesting platforms for oxygen reduction and hydrogen oxidation reactions. Using theoretical calculations, we show that such systems present markedly different catalytic behaviour from the known classes of materials.

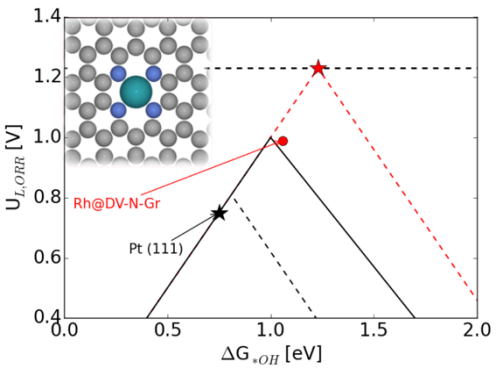

*Seoin Back, Ambarish R. Kulkarni, Samira Siahrostami**

Page No. – Page No.

Single Metal Atoms Implanted in Two-Dimensional Materials: Bifunctional Catalysts for Fuel Cell Application